© 2020. Published by The Company of Biologists Ltd | Journal of Cell Science (2020) 133, jcs238964. doi:10.1242/jcs.238964

TOOLS AND RESOURCES

Poji: a Fiji-based tool for analysis of podosomes and associated proteins

Robert Herzog[1], Koen van den Dries[2], Pasquale Cervero[1] and Stefan Linder[1,*]

ABSTRACT

Podosomes are actin-based adhesion and invasion structures in a variety of cell types, with podosome-forming cells displaying up to several hundreds of these structures. Podosome number, distribution and composition can be affected by experimental treatments or during regular turnover, necessitating a tool that is able to detect even subtle differences in podosomal properties. Here, we present a Fiji-based macro code termed 'Poji' ('podosome analysis by Fiji'), which serves as an easy-to-use tool to characterize a variety of cellular and podosomal parameters, including area, fluorescence intensity, relative enrichment of associated proteins and radial podosome intensity profiles. This tool should be useful to gain more detailed insight into the regulation, architecture and functions of podosomes. Moreover, we show that Poji is easily adaptable for the analysis of invadopodia and associated extracellular matrix degradation, and likely also of other micron-size punctate structures. This article describes the workflow of the Poji macro, presents several examples of its applications, and also points out limitations, as well as respective solutions, and adaptable features to streamline the analysis.

This article has an associated First Person interview with the first author of the paper.

KEY WORDS: Podosomes, Invadopodia, Actin, Myosin, Vinculin, LSP1, Macro, Fiji

INTRODUCTION

Podosomes are micron-sized, actin-based adhesion and invasion structures. Together with invadopodia of cancer cells, they form the subgroup of invadosome adhesions (Linder et al., 2011; Murphy and Courtneidge, 2011). Podosomes are formed in a variety of cell types, including macrophages (Linder et al., 1999), osteoclasts (Destaing et al., 2003), dendritic cells (Burns et al., 2001), endothelial cells (Moreau et al., 2003), neural crest cells (Murphy et al., 2011) and smooth muscle cells (Burgstaller and Gimona, 2005). Podosomes are defined by their multi-part architecture, with a core of F-actin containing regulators such as WASp (Linder et al., 1999) and the Arp2/3 complex (Linder et al., 2000), a discontinuous ring structure (van den Dries et al., 2013b) of adhesion plaque proteins such as vinculin and talin (Zambonin-Zallone et al., 1989), and a cap structure that contains actomyosin contractility regulators such as lymphocyte-specific protein 1 (LSP1) (Cervero et al., 2018) and supervillin (Bhuwania et al., 2012). Podosomes display a remarkably broad repertoire of functions, ranging from cell-matrix adhesion and extracellular matrix degradation, to antigen presentation and mechanosensing, and we refer to several reviews that cover these various aspects (Albiges-Rizo et al., 2009; Alonso et al., 2019; Destaing et al., 2011; Linder, 2007; Linder and Wiesner, 2015; Paterson and Courtneidge, 2018; van den Dries et al., 2014, 2019).

Of note, especially myeloid cells such as macrophages often form >500 podosomes per cell, making podosomes a prominent component of the actin cytoskeleton of these cells. Moreover, podosomes can vary in their appearance and composition, as exemplified by the two subpopulations of precursor (Evans et al., 2003) and successor podosomes (Bhuwania et al., 2012) formed in primary human macrophages, with precursors being larger and more dynamic, and also containing β-actin and LSP1, while the smaller and more stable successors feature α-cardiac actin and supervillin as prominent components (Cervero et al., 2018). Furthermore, podosome architecture is now recognized as quite complex (van den Dries et al., 2019), resulting in corresponding diversity in substructural localization of podosome components. Also, overexpression or depletion of podosome components sometimes shows only subtle effects on different parameters such as podosome size, number, interdistance, architecture or function. Collectively, these features necessitate the use of a tool that enables the analysis of a large set of relevant parameters in a statistically significant number of these structures and that is able to detect also subtle differences in podosome architecture and function.

The first steps of automated podosome analysis were published in Cervero et al. (2013), to determine podosome numbers and lifetime in macrophages, as these parameters are often affected by manipulation of key podosome components. Later that year, a tool to characterize the spatial distribution of fluorescently labelled proteins at podosomes was published (Meddens et al., 2013). This analysis is based on using microscopy images to create layers of segmentation masks on podosomes, and then connecting the measured intensity to a distance from podosome cores. A method to detect and characterize invadopodia using live-cell imaging was introduced in Berginski et al. (2014), by combining the localization information of invadopodia, detected as F-actin puncta, and their degradative ability, by loss of gelatin-based fluorescence. Proag et al. (2016) presented a method for the characterization and tracking of podosomes using live-cell microscopy, by identifying F-actin maxima and measuring their height using atomic force microscopy. This included the acquisition of data on fluorescence intensity variations of core and ring proteins over time, as well as the characterization of podosome size and geometry by radial intensity profile measurements. The measurement of podosome protein intensity profiles has also been used in super-resolution microscopy by Joosten et al. (2018).

[1]Institute for Medical Microbiology, Virology and Hygiene, University Medical Center Eppendorf, Martinistr. 52, 20246 Hamburg, Germany. [2]Department of Cell Biology, Radboud Institute for Molecular Life Sciences, Radboud University Medical Center, Geert Grooteplein Zuid 26-28, 6525 GA Nijmegen, The Netherlands.

*Author for correspondence (s.linder@uke.de)

R.H., 0000-0001-8613-6491; K.v.d.D., 0000-0002-7816-5206; P.C., 0000-0002-9417-7733; S.L., 0000-0001-8226-2802

Received 6 September 2019; Accepted 27 February 2020

Journal of Cell Science (2020) 133, jcs238964. doi:10.1242/jcs.238964

These published methods allow for better and faster analysis of podosome microscopy data. However, in most cases, they can only be used for a specific scientific question, as they do not include all parameters required for a thorough analysis of podosomes and podosome-forming cells. While the tool of Cervero et al. (2013) is limited to the determination of cell sizes and podosome numbers, Meddens et al. (2013) gathered information about the mean of all podosomes, but not about single podosomes or the podosome-containing cell. Berginski et al. (2014) analysed invadopodia number and size and their degrading ability, but not invadopodia composition. Finally, the tools used in Proag et al. (2016) and Joosten et al. (2018) gathered information on mean podosome architecture and protein localization, but did not connect this to overall cellular levels of proteins or to characteristics of single podosomes.

In order to integrate the analysis of all necessary podosome and cell parameters into a single tool, and to avoid time-consuming manual analysis, we have developed a semi-automatic tool that enables the simultaneous analysis of cell and podosome properties. This includes cell size and podosome number, as well as fluorescence intensity of labelled proteins in the entire cell and the combined podosome-covered area, and also of single podosomes in multi-colour fluorescence images (currently adapted to up to four different fluorescence channels). The tool is a Fiji-based macro that we named 'Poji' ('podosome analysis by Fiji'), which enables the analysis of all previously described parameters in images from fixed cells. By connecting detailed information on podosomes with general properties of the cell, this tool can be useful to gain more detailed insight into the regulation, architecture and functions of podosomes. Moreover, we show that it can be easily adapted for the analysis of invadopodia and invadopodia-associated matrix degradation as well.

RESULTS

Overview: workflow of the Poji macro

A schematic overview of the Poji macro is shown in Fig. 1A, with the corresponding microscopy images in Fig. 1B. To detect podosome cores, a reference staining, usually for F-actin by fluorescent phalloidin such as AlexaFluor-568-conjugated phalloidin, is required. This can be combined with antibody-based labelling of multiple additional podosome components. While analysis by Poji is conducted automatically, initiation of the macro requires user interaction.

Before starting Poji, the original microscopy data (Fig. 1B1) obtained by confocal microscopy are split into the individual fluorescence channels, which are saved in respectively named folders. This step is intentionally not included in the macro, as additional pre-processing steps prior to the actual analysis can be required. However, we also publish a script for optional automatic splitting of fluorescent channels and *z* planes. For implementing this step, and also for overall handling of the macro, please refer to the user guide (https://github.com/roherzog/Poji).

Following this set-up, Poji is started, offering a number of interfaces prior to analysis. These interfaces include, among others, the labelling of fluorescence channels, the adjustment of detection parameters, definition of selection sizes around podosomes, and the manual definition of cell and podosome cluster areas. Selection of only the cell outline (Fig. 1B2), which defines the area in which the macro conducts the analysis, is usually sufficient for cells like macrophages, which show homogeneous distribution of podosomes. For cell types with inhomogeneous distributions, including dendritic cells that form podosome clusters, endothelial cells that form podosome rosettes or osteoclasts that display podosome rings or belts (Linder et al., 2011), or for contracting cells with a pronounced actin cortex, it is recommended to additionally define the area of podosomes, to decrease the rate of false positives (see Fig. 6). Importantly, Poji enables the option to define several cell areas per image and several podosome clusters per cell. While the cell areas are analysed independently from each other, the podosome clusters inside the same cell will be automatically combined, to define the podosome-forming part of cells. These properties of the macro enable the analysis of several cells per image, limiting human bias and workload, and supporting optimal detection.

The parameters for optimal detection of podosomes, including the number of potential smoothing steps and the noise tolerance for the 'Find maxima' function in Fiji, have to be determined empirically. Smoothing of images leads to the equalization of potentially high-intensity differences between adjacent pixels and supports detection of the geometrical centre of podosomes. Noise tolerance is used as a threshold value for the 'Find maxima' function of Fiji to detect pixels that differ in fluorescence intensity from their neighbours. Optimal interplay of both values directly influences the quality of podosome detection and has to be carefully balanced. Therefore, Poji offers a preview function to facilitate optimization of detection parameters for individual cells. It has to be emphasized that individually adjusted detection parameters, leading to optimal podosome recognition, are more important to ensure comparability between different experiments, as opposed to keeping these parameters consistent throughout analysis and thus risking an increase of false-positive and false-negative rates. However, in contrast to the detection parameters, other settings should be kept as consistent as possible. This includes comparable microscopy settings prior to analysis and identical selection sizes around podosomes for profile analysis.

During the analysis, the Poji macro uses the fluorescence channel of the podosome core (here F-actin, stained with AlexaFluor-568-conjugated phalloidin) to measure fluorescence intensity (in grey values) and size of the cell area (in μm^2) (Fig. 1B3). In addition, the podosome core channel is used as a reference to determine the number and localization of podosomes, according to the individually adjusted detection parameters. A circular region of interest (ROI) of adjustable diameter (here 1.6 µm per podosome) is created around the centre of each podosome. Potentially overlapping ROIs are combined to prevent inclusion of duplicated pixels, and the sum of all ROIs is then copied to a new image, carrying the information of the cell area covered by podosomes (Fig. 1B4). The image of this podosomal area is then analysed for size and for fluorescence intensity by calculating the integrated density.

In addition to the collective podosomal area, the podosome ROIs are also analysed as single structures. The macro isolates all circular podosome ROIs and copies them to a stack of images, with one slice being the ROI of one individual podosome (Fig. 1B5). The podosomes are then successively analysed for fluorescence intensity, which is used to plot the distribution of intensity per podosome. Additionally, the Poji macro creates a second stack of single podosomes, isolated in square ROIs, that is subsequently merged into one image by performing a *z* projection that combines the average information of all podosomes into one slice (Fig. 1B6). The intensity profile of this *z* projection is measured across a diametrical line that is rotated 360 times for 1° each. The mean of all measurements is used to plot the average intensity against the distance of the profile line from the podosome centre (Fig. 1B7). The localization information on cell area, podosomal area and single podosomes is saved and re-used in the analysis of additional fluorescence channels. The fluorescence intensities on all three levels are measured by calculation of the integrated density, and,

Journal of Cell Science (2020) 133, jcs238964. doi:10.1242/jcs.238964

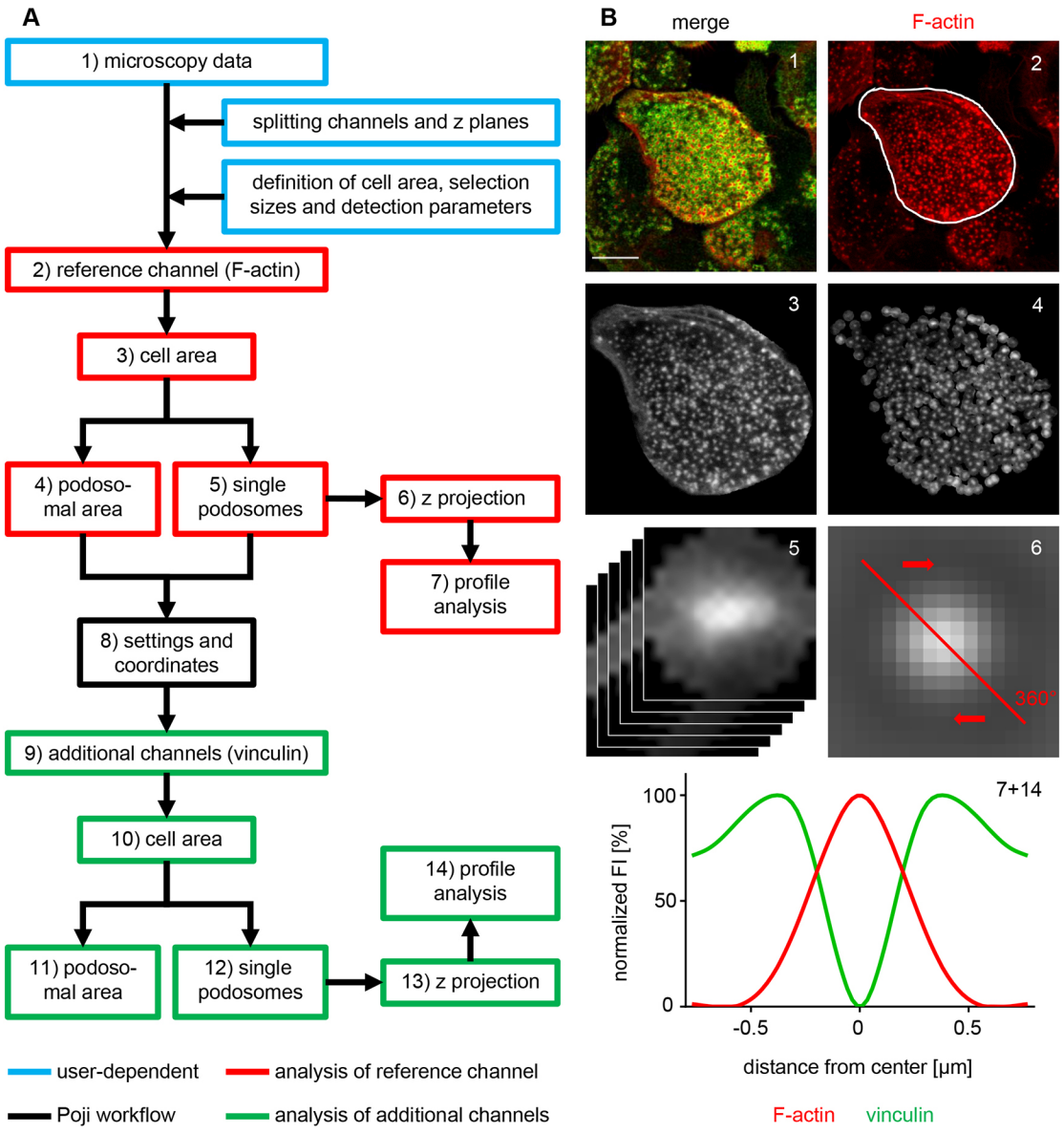

Fig. 1. Schematic overview of the Poji work flow. (A) Main processing steps of the macro. The original image (1) is split into the respective fluorescence channels, and settings such as noise tolerance, number of smoothing steps and cell area are defined prior to automated analysis (blue boxes; user-dependent steps). At the start of the automated analysis, the F-actin channel (2) is taken as a reference to automatically determine important cell parameters. In automated processes, the cell area is isolated to a new image (3), and the location and number of podosomes are identified by a maximum-intensity analysis. The combined area of all podosomes (4) is isolated and analysed separately. Additionally, podosomes are isolated as single structures to an image stack (5) and analysed successively (note that podosomes are copied in circular selections for intensity analysis and in square selections for the profile analysis). An average intensity *z* projection of the podosome stack is created (6), and the fluorescence intensity across a profile line is calculated (7). The selection coordinates (8) of cell and podosomal area, and also of single podosomes, are saved and used in the analysis of additional fluorescence channels (9–14). (B) Corresponding images of the main processing steps. Confocal laser-scanning micrographs of a primary human macrophage, stained for F-actin using AlexaFluor-568-labelled phalloidin, to visualize podosome cores, and co-stained for vinculin, using specific primary and AlexaFluor-488-conjugated secondary antibodies, as example for a podosome ring component (1). Shown are successive steps of the semi-automatic analysis (2–6) and from the profile analysis of the *z* projection of podosomes, giving the normalized fluorescence intensities for each channel (7,14), with profile graphs generated using cubic spline interpolation. Scale bar: 10 µm.

following the *z* projection of podosomes, the respective intensity profile of podosomes for these fluorescence channels is calculated. The measurements of all channels are saved separately and can be used in premade Excel tables that automatically calculate 19 different sets of data. For the Poji macro code, the analysis tables, a user guide and the code for automatic channel splitting, see https://github.com/roherzog/Poji.

In the following, we present several examples that illustrate the potential applications of Poji. The paper is structured in a way that we first show the ability of the macro to report fluorescence intensities and distribution of proteins in a single cell (Fig. 2), and then in multiple cells (Fig. 3), as well as in different *z* planes of podosomes (Fig. 4), and finally also for invadopodia in cancer cells (Fig. 5).

Application 1: changes in fluorescence intensity after myosin II inhibition

Actomyosin-dependent contractility is important for podosome turnover (Bhuwania et al., 2012), oscillations (van den Dries et al.,

Journal of Cell Science (2020) 133, jcs238964. doi:10.1242/jcs.238964

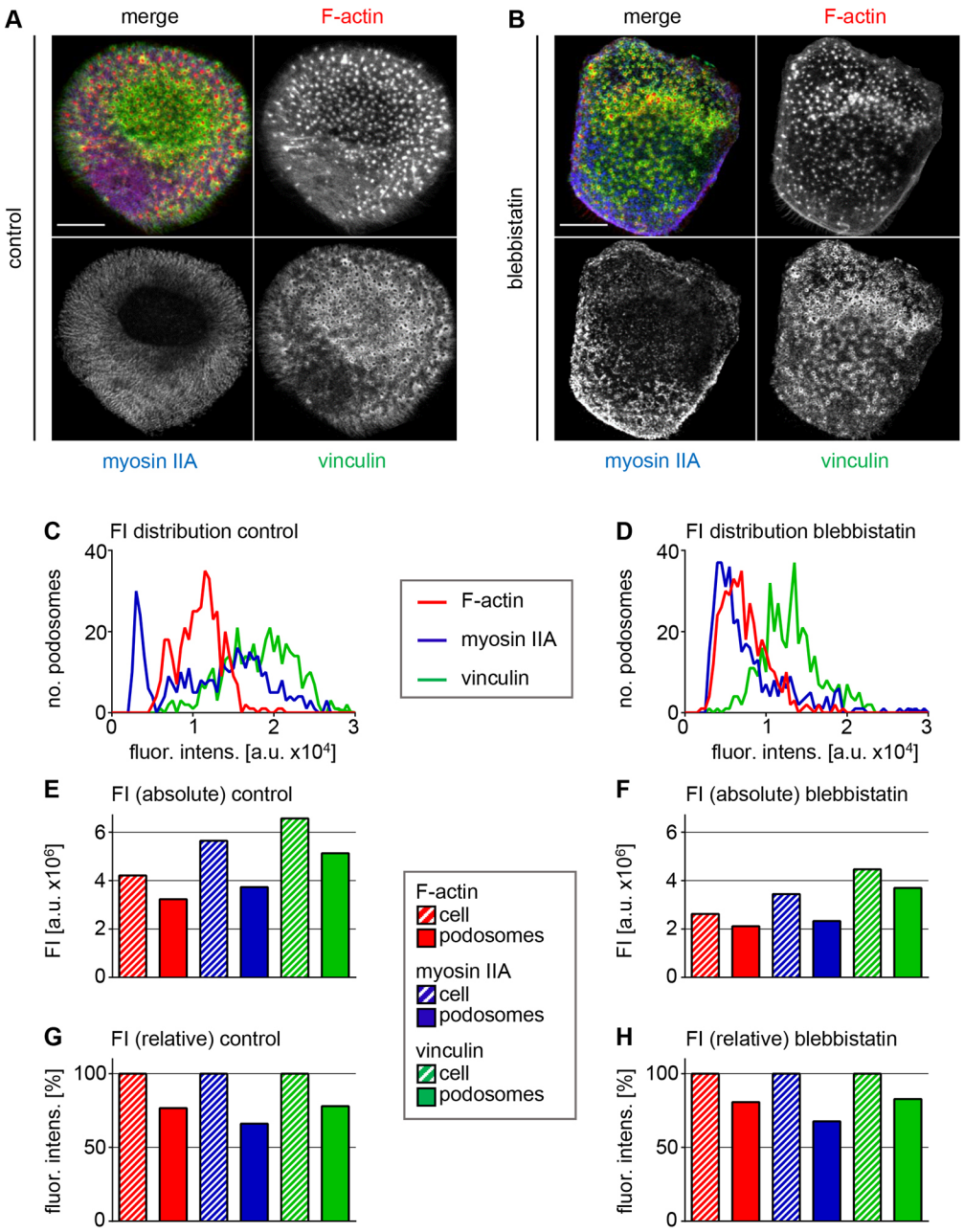

Fig. 2. Representative analysis after myosin IIA inhibition by blebbistatin. (A,B) Confocal micrographs of primary human macrophages treated with DMSO as a control (A) or with 10 µM blebbistatin for 30 min (B) and stained for F-actin using AlexaFluor-647-labelled phalloidin (upper right), and for myosin IIA (lower left) and vinculin (lower right), using specific primary and fluorescently labelled secondary antibodies (AlexaFluor-568 for myosin IIA, AlexaFluor-488 for vinculin). Coloured merges, with individual fluorescence channels shown in black and white. Images show cell area selection after Poji analysis. Scale bars: 10 µm. (C,D) Intensity distribution of single podosomes. Podosomes were binned with a fluorescence intensity interval of 500 arbitrary units (a.u.) per group. The number of podosomes within these groups was plotted against the corresponding level of fluorescence intensity for the control cell (C) and the blebbistatin-treated cell (D), respectively. (E–H) Fluorescence intensities for each channel, in the cellular and the combined podosomal area, were calculated and plotted for the control cell (E) and the blebbistatin-treated cell (F). Respective ratios, with cellular fluorescence intensity set to 100%, were calculated for the corresponding podosomal areas for both cells (G,H).

2013a) and podosome mechanosensing (Cervero et al., 2018). Accordingly, myosin IIA (also known as MYH9), the predominant myosin II isoform expressed in macrophages (Maupin et al., 1994), is closely associated with podosomes. In particular, it is part of the lateral actomyosin cables that previously have been shown to extend from the top of the podosome core towards the adhesive ring (Luxenburg et al., 2007), and is especially enriched at the dorsal connecting cables that organize podosomes into higher-ordered clusters (Luxenburg et al., 2007; van den Dries et al., 2019). Inhibition of the ATPase activity of myosin IIA by the inhibitor blebbistatin is thus a commonly used method to disrupt actomyosin contractility at podosomes, as it not only affects the mechanics of single podosomes, but also the connections between podosomes and the overall distribution of myosin IIA inside the cell.

To analyse the impact of blebbistatin treatment on myosin IIA localization at podosomes and in cells, 7-day-old primary human macrophages were treated with 10 µM blebbistatin for 30 min, fixed and stained for the core component F-actin, the ring component vinculin and myosin IIA, and samples were imaged by confocal microscopy. As described previously, the control cell showed a widespread and ordered distribution of myosin IIA throughout most of the cell area (Fig. 2A), whereas the striated pattern of myosin II was no longer visible in the blebbistatin-treated cell, and myosin II was mostly present at the cell periphery and the trailing edge of the cell, where podosomes are known to be dissolved by myosin II activity (Bhuwania et al., 2012) (lower part of cell in Fig. 2B). Moreover, whereas podosomes in the control cell seemed to be embedded in a striated network of myosin structures (Fig. 2A), myosin was mostly absent from the podosomal area (Fig. 2B). Of note, most of the myosin IIA in the cell periphery, although present in the podosomal area, is not an intrinsic component of podosomes, except the pool at the lateral and dorsal connecting cables (van den Dries et al., 2019). These pools can only be visualized at higher resolution.

Journal of Cell Science (2020) 133, jcs238964. doi:10.1242/jcs.238964

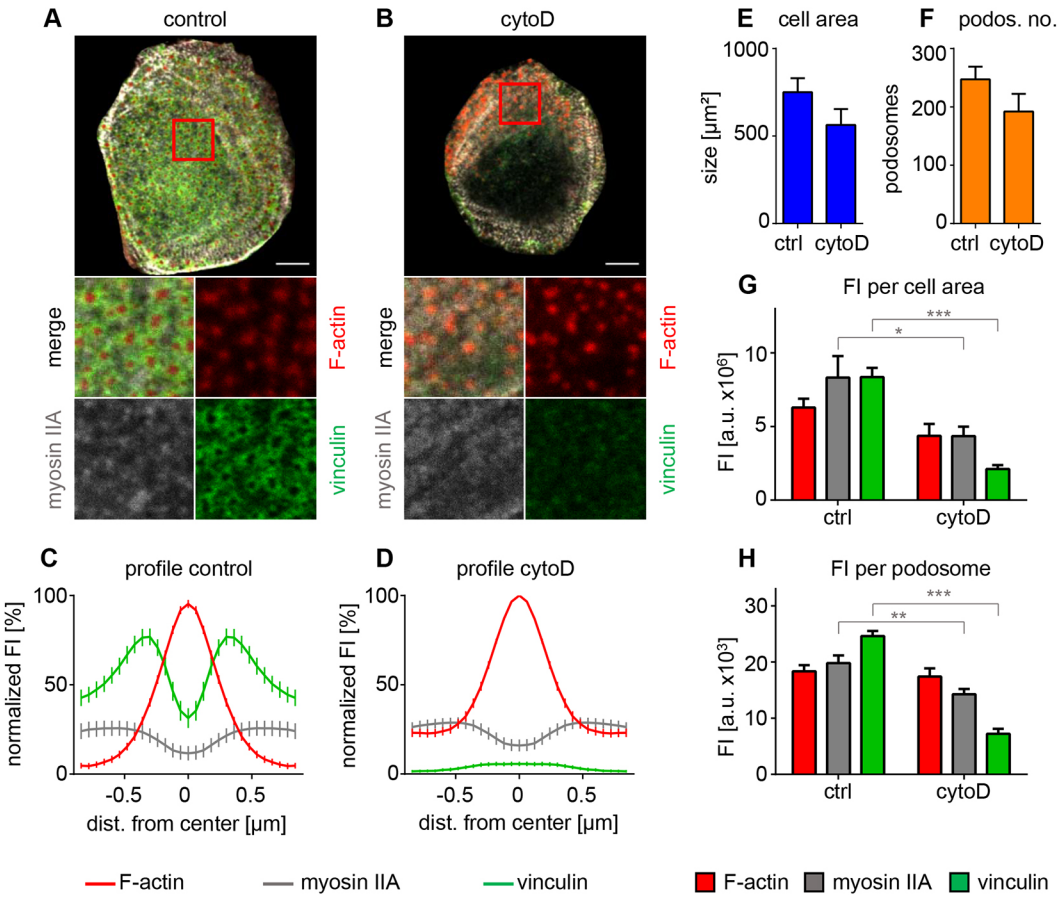

Fig. 3. Cytochalasin D treatment leads to loss of vinculin from podosomes. (A,B) Representative confocal micrographs of primary human macrophages, with a control cell treated with DMSO (A) and a cell treated for 10 min with 2 µM cytochalasin D (cytoD) (B). Cells were stained for F-actin (red) using AlexaFluor-647-labelled phalloidin, and for myosin IIA (grey) and vinculin (green) using specific primary antibodies and fluorescently labelled secondary antibodies (AlexaFluor-568 for myosin IIA, AlexaFluor-488 for vinculin), with merges. Red boxes indicate areas of detail images shown below. Images show cell area selection after Poji analysis. Scale bars: 5 µm. (C,D) Radial fluorescence intensity profiles of podosomes from control cells (C) or cytochalasin D-treated cells (D). Fluorescence intensity values for F-actin (red), myosin IIA (grey) and vinculin (green) were normalized to set the highest and lowest intensity value per cell to 100% and 0%, respectively. Shown are the mean±s.e.m. of at least 15 cells per condition. (E–H) Statistical evaluation of cell size (E), podosome number (F), overall cellular fluorescence intensities of F-actin, myosin IIA and vinculin (G), or fluorescence intensities at single podosomes of F-actin, myosin IIA and vinculin (H) in control cells and cells treated with cytochalasin D. Values are given as mean±s.e.m. from at least 15 cells per condition. *$P \leq 0.05$, **$P \leq 0.01$ and ***$P \leq 0.001$.

To correctly quantify this visible difference in myosin IIA localization using the Poji macro, the respective fluorescence intensity has to be measured at three levels, as described above: at single podosomes, in the total podosomal area and in the whole cellular area. The fluorescence intensity at single podosomes (see Fig. 1A, step 5) was automatically determined and binned in groups with a fluorescence intensity interval of 500 arbitrary units (a.u.) per group. After binning, a histogram with a number of podosomes within the binned groups, plotted against the intensity range of that group, was created for both the control and the blebbistatin-treated cell (Fig. 2C,D). Accordingly, two peaks are present in the myosin IIA distribution histogram of the control cell, one with a value of 3000–4000 a.u., representing podosomes in the area around the nucleus (Fig. S1), and also a second broader peak in the range of 8500–18,000 a.u., representing podosomes in the cell periphery (Fig. 2C). In contrast, the myosin IIA histogram of the blebbistatin-treated cell shows only one pronounced peak at a value of 4000–5500 a.u., reflecting the loss of the striated myosin IIA network in the cell periphery (Fig. 2D). The histograms of F-actin and vinculin in the control and the blebbistatin-treated cell show a similar pattern of intensity distribution, with the mean values of the control cell being slightly higher (Fig. 2C,D), due to a generally higher level of fluorescence intensity in the control cell within both cellular and podosomal areas (see Fig. 1A, steps 3 and 4), in comparison to the blebbistatin-treated cell (Fig. 2E,F). Interestingly, the ratio of intensities in the podosomal versus the overall cellular area (set to 100% in each channel) is similar in both cells (Fig. 2G,H), indicating that the observed difference in intensity distribution at podosomes is likely due to cellular changes instead of individual composition changes at podosomes. The Poji macro is thus not only able to measure intensities at single discrete levels (podosome, podosomal area, cellular area), but also to combine this information to assess whether changes in fluorescence intensities are due to specific alterations in podosome composition or to overall changes in the cell.

Application 2: analysis of vinculin localization after cytochalasin D treatment

The above-described example shows that the Poji macro can extract a set of cellular and podosomal parameters from images of single cells. This analysis can be extended for multiple cells and different treatments. Accordingly, we analysed the impact of cytochalasin D, an inhibitor of actin filament elongation (Sampath and Pollard, 1991). Primary macrophages were treated with DMSO for controls

Journal of Cell Science (2020) 133, jcs238964. doi:10.1242/jcs.238964

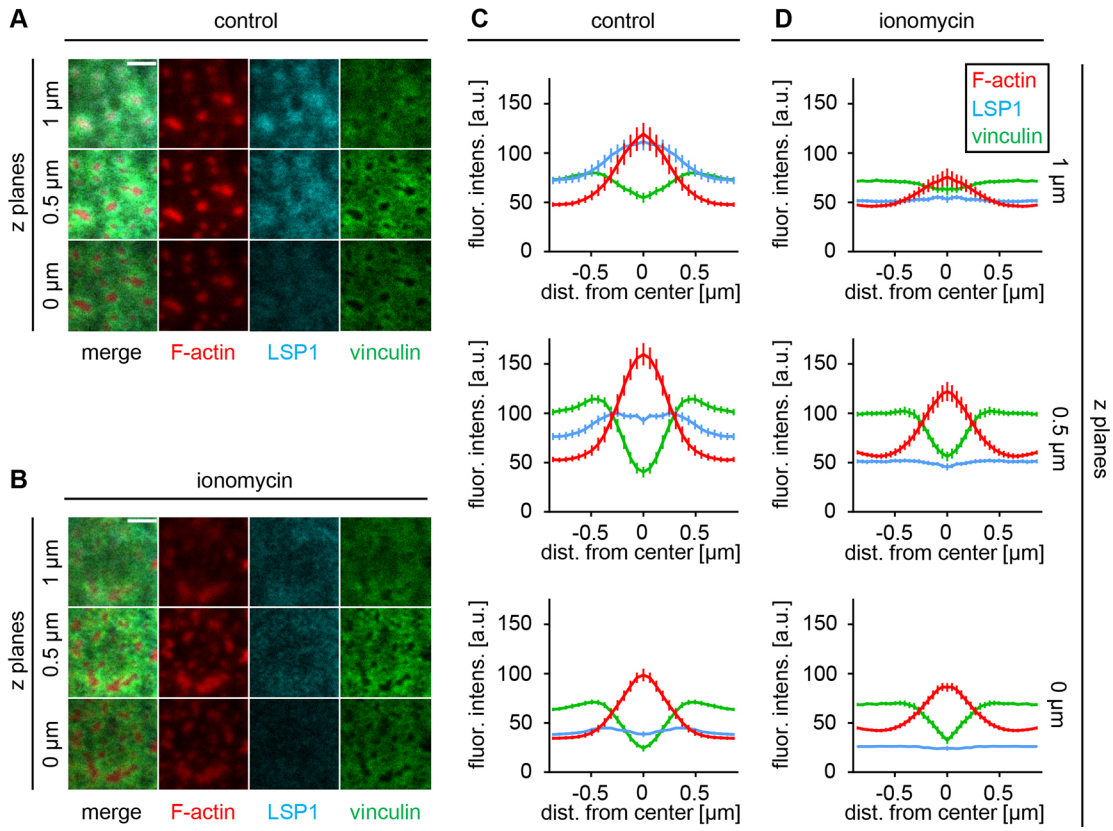

Fig. 4. Ionomycin treatment leads to loss of LSP1 from the podosome cap. (A,B) ROI from confocal micrographs of macrophage podosomes in a control cell treated with DMSO (A) and a cell treated for 10 min with ionomycin (2 µM) (B). For full confocal images, see Fig. S2. Cells were stained for F-actin using AlexaFluor-647-labelled phalloidin (red), and for LSP1 (cyan) and vinculin (green) using specific primary antibodies and fluorescently labelled secondary antibodies (AlexaFluor-568 for LSP1, AlexaFluor-488 for vinculin). Podosomes were visualized at *z* distances of 0 µm, 0.5 µm and 1 µm from the ventral sides of cells. Scale bars: 2 µm. (C,D) Radial fluorescence intensity profiles for F-actin (red), LSP1 (cyan) and vinculin (green) of podosomes in ROIs of control (C) and ionomycin-treated (D) cells. Profiles were calculated for all podosomes in ROIs of both cells individually, with mean±s.e.m. of projections of all podosome profiles shown [at *z* planes of 1 µm, 0.5 µm and 0 µm distance to the most ventral F-actin signal of podosomes; *n*=16 podosomes (control) and *n*=22 podosomes (ionomycin) per *z* section]. Note loss of LSP1 from the podosome cap upon treatment with ionomycin (C,D). For images and analysis of complete control and ionomycin-treated cells, see Fig. S2.

(Fig. 3A) or with 2 µM cytochalasin D (Fig. 3B) for 10 min, stained for F-actin, myosin IIA and vinculin, and imaged by confocal microscopy.

Poji was used to create fluorescence intensity profiles for the average of all podosomes of each cell. Profiles were normalized, by setting the highest and lowest fluorescence intensity value for all channels to 100% and to 0% per cell, respectively. The mean of all cells per condition (n>3000 podosomes from ≥15 cells per condition) was calculated to highlight the relative changes in podosome composition that were induced by cytochalasin D treatment. As already visible in the fluorescence images (Fig. 3A,B), cytochalasin D led to pronounced loss of vinculin

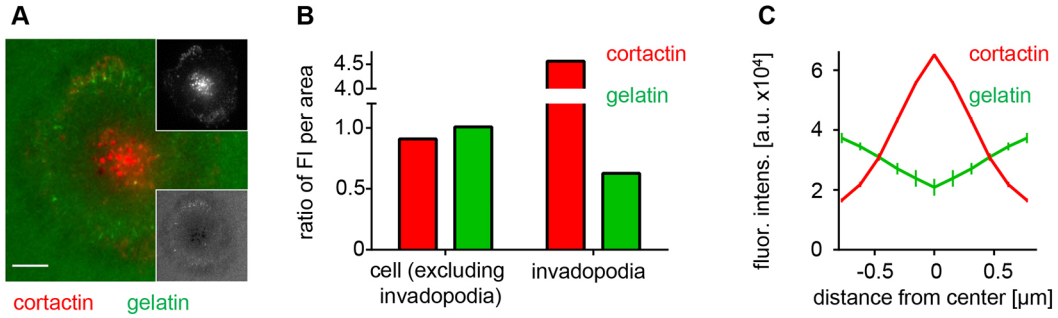

Fig. 5. Gelatin degradation by invadopodia. (A) Confocal micrograph of an MDA-MB 231 cell, stained for cortactin (red, upper inset) and seeded on FITC-labelled gelatin (green, lower inset), according to Monteiro et al. (2013). Scale bar: 10 µm. (B) Distribution of fluorescence intensity per cell area without invadopodial area or per invadopodial area. Fluorescence intensities divided by respective total cellular fluorescence intensity were compared to the size of these areas divided by entire cell area. Respective ratios are shown for both cortactin and gelatin, with 1.0 indicating uniform distribution. (C) Average radial fluorescence intensity of detected invadopodia, shown by dot-like cortactin distribution. Gelatin degradation is visible by decrease in the normalized fluorescence intensity, especially at the centre of invadopodia. Shown is the mean±s.e.m. of 28 invadopodia.

Journal of Cell Science (2020) 133, jcs238964. doi:10.1242/jcs.238964

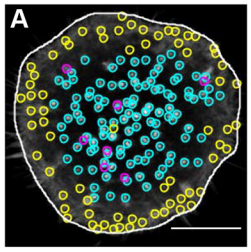

entire cell area	no. of podosomes	overlap with Expert 1	overlap with Expert 2	overlap with Expert 3	overlap with Poji
Expert 1	115	xxx	101	104	108
Expert 2	104	101	xxx	103	103
Expert 3	108	103	102	xxx	103
Poji	180	107	103	103	xxx

Poji perfomance	confirmed by experts:	false positives:	false negatives:
	111 (62%)	69 (38%)	7 (4%)

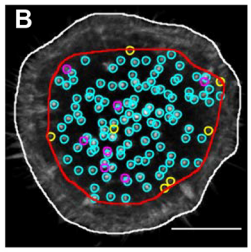

podosome cluster	no. of podosomes	overlap with Expert 1	overlap with Expert 2	overlap with Expert 3	overlap with Poji
Expert 1	115	xxx	101	104	108
Expert 2	104	101	xxx	103	103
Expert 3	108	103	102	xxx	103
Poji	118	107	103	103	xxx

Poji perfomance	confirmed by experts:	false positives:	false negatives:
	111 (94%)	7 (6%)	7 (6%)

Fig. 6. False positives and false negatives. (A,B) Non-podosomal F-actin maxima. Confocal micrograph of primary macrophage stained for F-actin using AlexaFluor-568-labelled phalloidin, with analysed ROI (white border) encompassing the entire cell (A) and with additional restriction to the podosome-forming part of the cell (red border) (B), as determined by visual control. Images show cell area selection after Poji analysis. Scale bars: 10 µm. Note that the number of false positives (yellow circles) is reduced from 38% in A to 6% in B, without altering the number of detected bona fide podosomes, as confirmed through visual control by three independent experts (blue circles). The absolute number of false negatives (magenta circles) is mostly unchanged, but their relative abundance is increased from 4% in A to 6% in B, due to the lower number of detected F-actin maxima.

from podosomes, whereas the overall distribution of F-actin and myosin IIA at podosomes was mostly unaffected (Fig. 3C,D). Moreover, cytochalasin D led to non-significant reductions in cell size by 25% (Fig. 3E) and in podosome numbers by 23% (Fig. 3F). Analysis of fluorescence intensities showed that, in the ventral plane used for confocal imaging, values for myosin IIA and vinculin were significantly decreased, with vinculin especially showing a strong reduction, by 75% (Fig. 3G). By contrast, F-actin intensity levels showed only a slight decrease. Furthermore, analysis of protein levels per podosome showed that, in contrast to overall cellular levels, F-actin intensities were not reduced, whereas both myosin IIA and vinculin showed a significant reduction (Fig. 3H) that mirrored their overall reduction at the ventral part of cells (Fig. 3G).

Collectively, this analysis confirms the previously reported general effect of cytochalasin D on vinculin localization at podosomes (van den Dries et al., 2013a) and extends this further, by adding detailed quantifications of fluorescence intensity changes, also of other podosome-associated proteins.

Application 3: analysis of LSP1 in different confocal planes after ionomycin treatment

The podosome cap extends from the top of the core along the sides of podosomes. Depending on the plane of imaging, it can thus appear as a dot or as a ring. Analysis of cap-localized proteins thus requires imaging of different and multiple confocal planes, as opposed to imaging of the core or the ring. LSP1 is a recently described cap component that regulates podosome oscillatory protrusion (Cervero et al., 2018). To visualize LSP1 at podosomes, human macrophages were stained for F-actin, vinculin and LSP1, and localizations of these proteins at podosomes were visualized using confocal microscopy in three different optical planes, at 1, 0.5 and 0 µm z distance from the most ventral F-actin signal (Fig. 4A). While LSP1 is located in the centre of the podosome at the highest focal plane (1 µm), it is organized more into a ring-like structure at the lower z planes (0.5 µm, 0 µm). By contrast, the localization of F-actin and vinculin per se does not change, and only changes in overall fluorescence intensities are detected.

The Poji macro was used to plot intensity profiles of LSP1 in all three confocal planes. In contrast to prior analyses, where profiles were generated just once after all podosomes were merged into one image by average intensity z projections (see Fig. 1A, step 6), the profiles in this application were created for all podosomes inside the selected ROI individually, with the mean±s.e.m. of all profiles shown in Fig. 4C,D. This step ensures that the heterogeneity of podosomes is preserved in the analysis and displayed through the error bars. Accordingly, LSP1 shows the highest fluorescence intensity in the highest focal plane (z=1 µm) at the centre of the podosome, which is decreasing towards the periphery, thus corresponding to a dot-like localization on top of the podosome core (Fig. 4C). At z=0.5 µm, LSP1 localization shows a local intensity minimum at the podosome centre. In addition, the vinculin ring structure is clearly detectable at this plane (Fig. 4C). In the lowest plane (z=0 µm), the maximum intensity of the LSP1 profile is present at a lateral distance of 0.3 µm to the centre of the podosome, with an even more pronounced local minimum in the centre of the podosomes, corresponding to a more ring-like distribution (Fig. 4C). At the same time, LSP1 is still more closely associated with the core compared to vinculin, as vinculin has its highest intensity at a lateral distance of 0.5 µm, corresponding to the radius of the podosome ring. Of note, the general bipartite distribution of vinculin is preserved also at the focal planes of z=0 µm and z=0.5 µm, clearly reporting its consistently ring-like localization, which is in clear contrast to the changing distribution of LSP1 across planes of imaging. Finally, the profiles of F-actin are similar in all confocal planes, the only difference lying in the absolute intensities (Fig. 4C). Moreover, the relative intensities of each visualized protein also indicate the respective enrichment in a confocal plane, with LSP1 being especially prominent at the highest confocal plane (z=1 µm), and vinculin enriched at the lower planes (z=0.5 µm, z=0 µm). Of note, the difference in LSP1 localization in several

Journal of Cell Science (2020) 133, jcs238964. doi:10.1242/jcs.238964

optical planes has been shown in an ROI here. However, the average result of all podosomes of the cell can partially mask this heterogeneous recruitment, as podosomes, especially those of different subtypes (precursors, successors), can vary in height. For results of the whole cell, see Fig. S2.

It is currently unclear whether cap proteins such as LSP1 are associated constantly with podosomes during their life cycle, and, if so, which consequences ensue for podosome composition and function. We thus asked whether the association of LSP1 with podosomes can be influenced pharmacologically, comparable to the loss of vinculin due to cytochalasin D treatment, as described above. From several chemical inhibitors that we tested, the clearest effect was obtained upon the use of ionomycin, a Ca^{2+} ionophore (Liu and Hermann, 1978). Treatment of primary macrophages for 10 min with 2 µM ionomycin led to a loss of LSP1 from podosomes in all respective confocal planes (Fig. 4B). At the same time, F-actin and vinculin were still present at podosomes, indicating the integrity of both core and ring structures (Fig. 4B). Poji-based plotting of intensity profiles of all three proteins confirmed this, as both F-actin and vinculin showed their typical distribution, although at slightly reduced values, especially at the confocal planes (z=0.5 µm, z=1 µm), with a central enrichment of F-actin and a bipartite enrichment of vinculin at lateral peaks of ∼0.5 µm from the podosome centre (Fig. 4D). By contrast, LSP1 no longer showed a specific enrichment at podosomes at any of the three confocal planes (Fig. 4D), pointing to its complete loss from the structure. The loss of LSP1 is also reflected in the average profile of all podosomes from this cell (Fig. S2).

This is the first indication that a podosome cap protein can be selectively removed by pharmacological means. Poji-based analysis of several confocal planes thus appears to be particularly suitable for the investigation of podosome cap proteins.

Application 4: detection of invadopodia and associated matrix degradation

We next investigated whether Poji is suitable for the detection and analysis of invadopodia and associated sites of extracellular matrix degradation. Images of invadopodia-forming MDA-MB-231 breast cancer cells seeded on fluorescently labelled gelatin matrix were kindly provided by Dr Pedro Monteiro and Dr Philippe Chavrier (Institut Curie, Paris, France). Invadopodia were detected by staining cells for the cortactin, while gelatin was labelled by fluorescein isothiocyanate (FITC) [for details, see Monteiro et al. (2013)] (Fig. 5A). In contrast to the F-actin based analysis of macrophage podosomes, invadopodia were analysed using the cortactin channel as a reference.

Analysis of cortactin- and gelatin-based fluorescence intensities showed that, in comparison to the total cellular area (excluding invadopodia), cortactin was enriched ∼5× in the invadopodial area, whereas gelatin-based fluorescence was decreased by ∼50% (Fig. 5B). Moreover, analysis of the normalized cortactin- and gelatin-based fluorescence intensities showed that the peak of cortactin fluorescence in the centre of invadopodia corresponded to a local minimum of gelatin-based fluorescence, indicating a close correlation between the invadopodial core and invadopodia-associated matrix degradation (Fig. 5C). Collectively, this application shows that Poji should also be a useful tool for the analysis of invadopodia and invadosome-associated areas of matrix degradation in general.

Limitations and solutions: avoiding potential pitfalls when using the Poji macro

Despite the versatility of the Poji macro, certain limitations have to be kept in mind. Most importantly, the tool localizes podosomes on the basis of local maximum intensity, usually of F-actin, with the noise tolerance being defined manually. Adjusting noise tolerance (in combination with the optimal number of smoothing steps) to obtain the best results may thus be the most time-consuming part when using the tool. Still, even correctly identified local maxima in F-actin based fluorescence do not necessarily represent podosomes. In most cases, using monocytic cells such as macrophages, this does not pose a problem, as podosomes represent the major part of the actin cytoskeleton in these cells. However, in other cell types like dendritic cells, or cells showing a more pronounced cortical actin cytoskeleton such as in contracting macrophages, non-podosomal F-actin maxima can be more prominent. This leads to a misidentification of F-actin maxima especially in the cell periphery. It is thus advisable to restrict the area of podosome detection to only the truly podosome-forming part of the cell. The Poji macro enables this restriction, without limiting the analysis of the entire cell area, by offering the option to additionally select a podosome cluster area in which podosomes are detected. The percentage of false positives can thus be strongly reduced. In the example shown, false positives were reduced from 38% to 6%, while the number of false negatives increased slightly from 4% to 6%, due to less local F-actin maxima being included in the analysis (Fig. 6A,B). Note that while podosome number is directly influenced by the additional selection of a cluster area, other parameters like cell size and cellular fluorescence intensity are not influenced, as the analysed cell area is not altered.

Inadequate settings for image acquisition, especially resolution and zoom, as well as inadequate processing steps, adjusted in the interface steps of the Poji macro (see https://github.com/roherzog/Poji), can lower the tool's ability to correctly identify podosomes. Adequate smoothing of the podosome-defining F-actin channel, which replaces each pixel with the average of its 3×3 pixel neighbours, is particularly important in this context. As the macro defines podosomes as local maxima of fluorescence intensity, podosome definition in a non-smoothed image could lead to the highest intensity pixel being placed centrally, although it does not correspond to the real centre of the podosome. This could lead to artefacts, especially in the generation of podosome profiles, as the intensity of the central pixels would be disproportionally high, thus leading to a non-representative profile of the podosome core (Fig. 7A,B). Of note, this artefact is limited to the F-actin channel used for initial detection of podosomes, and average profiles of vinculin, for example, are not comparably affected (Fig. 7B). Smoothing of the image prior to detection leads to a more reliable recognition of the centre of podosomes, thus resulting in more-representative profiles (Fig. 7A,B). Note that the smoothing steps for the podosome detection are not performed in the images of the analysis, but in automatically generated duplicates, so that smoothing only has an impact on the detection performance of the macro, but does not alter the original data.

It should also be mentioned that the macro averages certain data points during the analysis, leading to the loss of individual differences in podosome appearance or composition, and thus affecting especially the profiles of the average intensity projection. Differences in podosome shape or composition (Fig. 7C), for example due to fusion or fission processes (Evans et al., 2003; Kopp et al., 2006), or based on the existence of distinct podosome subpopulations such as the precursors and successors in primary human macrophages (Bhuwania et al., 2012; Cervero et al., 2018; Evans et al., 2003), could thus be overlooked. For examples of these individual differences in podosome size and fluorescence intensity distribution, see Fig. 7C–E and compare them to the average of all

Journal of Cell Science (2020) 133, jcs238964. doi:10.1242/jcs.238964

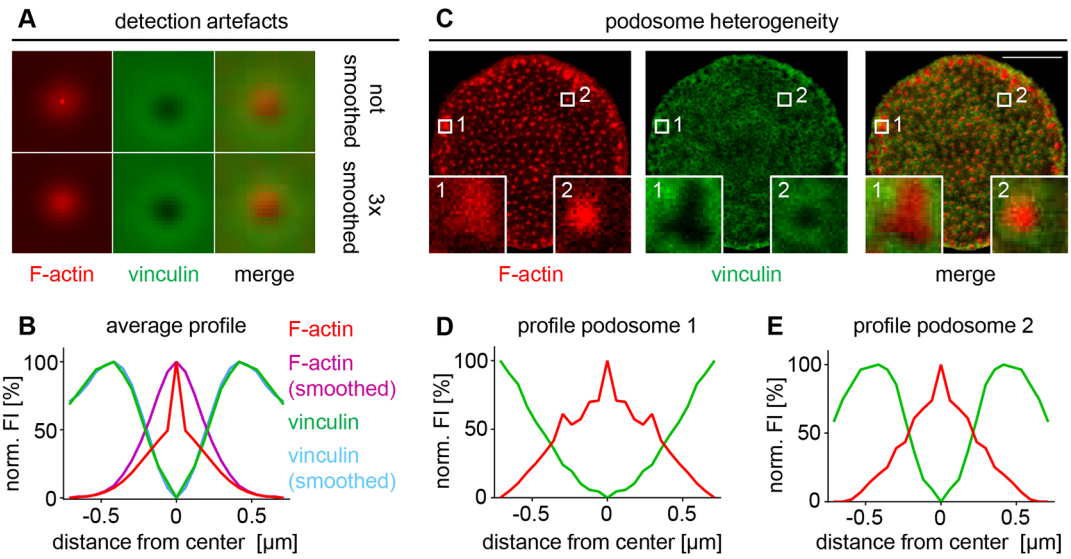

Fig. 7. Technical limitations of the tool and possible solutions. (A,B) Artefacts in average profiles due to inadequate settings. (A) Average intensity *z* projections of all podosomes of the cell shown in C for F-actin, vinculin and merge. Profiles were not smoothed (upper row) or smoothed 3× (lower row) prior to podosome detection. (B) Intensity profile analysis of the *z* projection of all podosomes of both F-actin (red) and vinculin (green). Note exaggerated intensity of central pixels in the F-actin channel used for detection of local maxima, leading to a miscalculation in the profile analysis. This can be addressed by including an adequate number of smoothing steps, offered by the macro, prior to podosome detection. This leads to a more even distribution of fluorescence in the average *z* projection (A) and thus to a more representative profile for F-actin (magenta) (B). Note that the fluorescence profile for vinculin (blue) is largely unchanged, as it is not used for the initial detection of the central maximum for podosome detection. (C–E) Heterogeneity of podosomes. (C) Confocal microscopy images of a primary human macrophage stained for F-actin, using AlexaFluor-568-labelled phalloidin (red), and vinculin, using specific primary and AlexaFluor-488-conjugated secondary antibodies (green), with merge. Scale bar: 10 µm. Images show cell area selection after Poji analysis. Numbered white boxes indicate respective detail areas shown enlarged in lower left and right. (D,E) Intensity profile analysis of individual podosomes shown in 1 and 2, respectively, showing differences in size and protein distribution of single podosomes in the same cell.

podosomes from this cell in Fig. 7B. For correct assessment of these differences, other data such as the fluorescence intensity distribution within a podosome population (Panzer et al., 2016) have to be taken into account. Furthermore, the Poji macro enables the option to not only analyse the average intensity *z* projection of all podosomes, but to additionally analyse the profiles of single podosomes in subsequent steps (as in Application 3 and 4; see also Fig. 1A, steps 5 and 6). Choosing either option depends on the specific scientific question being asked.

Furthermore, the Poji macro generates podosome intensity profiles by rotating the respective profile line 360 times in 1° steps (Fig. 1B6). As each pixel is thus measured twice, this results in mathematically symmetrical profiles, even when the actual structure is non-symmetrical (compare positions of F-actin core and vinculin ring in Fig. 7A with profiles in Fig. 7B). In the example presented, the ring structure is thus slightly off-centre in the confocal image, while it is placed directly underneath the centre of the core in the profile graph. This step was implemented despite the described ensuing limitations. This is mostly due to the fact that a rotation by only 180° would produce a different profile for the analysis of the same cell, depending on the orientation of the coverslip in the microscope, or on the direction of profile line rotation (clockwise versus counter-clockwise), thus leading to artificial differences.

DISCUSSION

Here, we present a Fiji-based macro code termed ‘Poji’, which serves as an easy-to-use tool to characterize a variety of cellular and podosomal parameters, including area, fluorescence intensity and relative enrichment of associated proteins. It should be useful to assess podosome number, distribution and composition in various cell types. Poji builds on features previously introduced for podosome analysis by several semi-automated tools (Cervero et al., 2013; Joosten et al., 2018; Meddens et al., 2013; Proag et al., 2016). However, it additionally incorporates further parameters such as overall cellular fluorescence intensity or analysis of single podosomes, and merges them into a coherent whole, allowing fast and comprehensive analysis of both podosomes and podosome-forming cells.

Adaptable parameters include, among others, (1) the number of smoothing steps prior to analysis and the definition of noise tolerance, which is important to detect single podosomes over the F-actin background, and which may differ based on the signal-to-noise ratio of individual images; and (2) the predefined area around podosomes in which fluorescence intensity is measured. By changing these values, the analysis can be adapted to changes in podosome size and according to different magnifications used for image acquisition. The entire image and the *z* profile projection can be analysed without any pre-processing steps to identify changes in intensity, or they can be automatically normalized prior to analysis to obtain comparable results, independently of differences in intensity. Normalization is performed by automatically adjusting each pixel’s intensity value to the maximum bit range. Supported bit depths of the macro are 8- and 16-bit images. Any unsupported image (e.g. 32-bit or RGB images) returns an error message and has to be adjusted to the 8- or 16-bit range.

We present several applications that illustrate the features of Poji in cell and podosome analysis. For example, treatment of macrophages with the myosin II inhibitor blebbistatin illustrates that Poji can be used to measure fluorescence intensities at different levels, including podosomes, podosomal area and cellular area, as well as distribution of specific proteins at single podosomes. Moreover, combining this information can be used to assess whether changes in fluorescence intensities are due to alterations in podosome composition or to overall cellular changes. Of note,

Journal of Cell Science (2020) 133, jcs238964. doi:10.1242/jcs.238964

podosome-associated myosin IIA is mostly present with the lateral and dorsal connecting cables (Bhuwania et al., 2012; van den Dries et al., 2019), and is thus located at a higher level, compared to the one used for localization of vinculin and F-actin (Fig. 2). For an assessment of the myosin IIA pool that is specifically associated with podosome cables, a confocal plane more distal to the substratum should be chosen.

The mostly inhibitory role of myosin II in podosome turnover is illustrated by the fact that macrophage podosomes show strongly increased levels of the myosin II hyperactivator supervillin, and also of myosin IIA, prior to their dissolution (Bhuwania et al., 2012). In contrast to this inhibitory role in podosome formation, more subtle changes in myosin II activity appear to contribute to podosome function. Accordingly, myosin II inhibition has been shown to decrease podosome oscillation in dendritic cells (van den Dries et al., 2013a) and macrophages (Panzer et al., 2016), and also disrupt the periodic cycles of podosomes stiffness in macrophages (Labernadie et al., 2010). Of note, these data are based on analysis of podosome numbers, association of myosin-regulatory proteins to podosomes and changes of protein distribution in the cell area upon pharmacological treatments. All of these analyses are now possible in larger numbers and at higher speed by using Poji, which should facilitate further insights into actomyosin contractility at podosomes.

In a second example, we investigated the influence of cytochalasin D, an inhibitor of actin polymerization, on various cellular and podosomal parameters. Analysis by Poji showed that addition of 2 µM cytochalasin D to cells led to slight reductions in cell area and in the number of podosomes. This was accompanied by a general reduction in the levels of F-actin, myosin IIA and vinculin at the ventral cell side. However, the loss of vinculin was even more pronounced, compared to F-actin and myosin IIA. Indeed, analysis of podosome-associated fluorescence showed that vinculin levels at podosomes were especially reduced, by ∼70%. In addition, we measured a ∼25% reduction in myosin IIA levels at podosomes. These results are in line with a previous report (van den Dries et al., 2013a), which showed that inhibition of podosome core growth by cytochalasin D led to reduced recruitment of vinculin and zyxin to the podosome ring structure in dendritic cells. This paper was crucial in establishing the role of podosome core growth as a myosin-independent force transduction system for the recruitment of tension-sensitive adaptors to the podosome ring. The Poji-based analysis presented here both confirms and extends these findings. Our quantifications show that vinculin levels are indeed strongly reduced at podosomes. However, myosin IIA levels are also slightly, but significantly, reduced at podosomes, pointing to a more complex interplay of actin core growth and myosin-based contractility in podosome mechanotransduction than assumed previously.

A third example, localization of the podosome cap component LSP1, is presented to illustrate the fact that not all podosomes proteins are located in the same focal plane. Here, the Poji macro is used to generate respective intensity profiles to illustrate the relative enrichment of core (F-actin), ring (vinculin) and cap components (LSP1) in different optical planes. Of note, LSP1 and supervillin are both components of the podosome cap and are both associated with myosin II, but they are differentially distributed in cells, with LSP1 being mostly localized to precursors (Cervero et al., 2018) and supervillin being mostly associated with successor podosomes (Bhuwania et al., 2012). This is based on the preference of LSP1 for binding of β-actin, which is enriched in precursors, resulting in a reciprocal association of supervillin with α-actin-rich successors (Cervero et al., 2018). We now show that the localization of LSP1 to the podosome cap structure can be influenced pharmacologically. Addition of the Ca^{2+} ionophore ionomycin to macrophage cultures led to complete loss of LSP1 from the podosome cap, while core and ring structures remained intact, as evidenced by the respective localization of F-actin and vinculin. This is the first report that a cap protein can be selectively removed from podosomes, and also that podosome architecture can be influenced by ionomycin. Generally, the influence of Ca^{2+} ions on podosome formation has been known for decades, with early reports showing that treatment with ionomycin (Teti et al., 1989) or addition of extracellular Ca^{2+} (Miyauchi et al., 1990) leads to reduced formation of podosomes in chicken osteoclasts. Moreover, a plethora of Ca^{2+}-regulated proteins are known to localize to podosomes, including caldesmon (Yoshio et al., 2007), calponin (Gimona et al., 2003) and gelsolin (Akisaka et al., 2001), among others. Many of these Ca^{2+}-regulated proteins are components of the podosome core structure. Therefore, the finding that the cap component LSP1 can be removed by ionomycin, while the core apparently remains intact, raises some intriguing questions. Are components of the podosome cap, being localized to the outer layers of podosomes, more easily removed than components of the core? Is only a subset of Ca^{2+}-regulated proteins dislocalized from podosomes upon ionomycin treatment and, if so, which proteins does this include? And finally, how does this impact on podosome functions such as mechanosensing or matrix degradation? The Poji macro should be particularly helpful in systematically addressing these questions and thus gaining more in-depth knowledge on the connections between podosome architecture, composition and functions.

In a fourth example, we demonstrate that Poji can also be used for the analysis of cancer cell invadopodia and to correlate them with areas of extracellular matrix degradation. Here, invadopodia of MDA-MB-231 breast cancer cells and associated regions of loss of FITC-labelled gelatin were analysed. Invadopodia were detected by cortactin-based fluorescence, as this component was prominently enriched at invadopodia (Monteiro et al., 2013), in contrast to F-actin, which was also enriched at other structures such as the actin cortex. At the same time, this application shows that the reference channel is not necessarily restricted to using F-actin-based fluorescence, but should be chosen by its suitability to selectively detect the structures of interest. This example clearly shows that Poji can be useful for the analysis of invadopodia and also of invadosome-associated matrix degradation in general. Moreover, extending the application of Poji to other dot-like cellular structures such as the podosome-associated metalloproteinase islets (El Azzouzi et al., 2016), or to actin foci of immunological synapses (Kumari et al., 2020), appears to be entirely feasible.

In conclusion, we present here a versatile and easy-to-use macro that is able to calculate and integrate a variety of podosomal and cellular properties. Apart from regular parameters such as cell size and podosome or invadopodia numbers, and from correlating invadosomes with respective areas of matrix degradation, the tool is also able to detect even subtle differences in cellular and podosome composition due to various treatments or environmental conditions. While the tool parameters need to be adapted and optimized for each analysed cell, it enables the analysis of statistically relevant numbers of cells and invadosomes. Still, it should be kept in mind that the individual variety between podosomes is higher than average values or profiles can depict. It is thus possible that individual differences, for example indicating podosome subgroups, are masked by use of the macro. Despite having a human bias, the well-honed eye of a researcher thus remains a vital resource that cannot be fully replaced by even the best tool.

MATERIALS AND METHODS

Isolation, seeding and culturing of macrophages

Human peripheral blood monocytes were isolated from buffy coats [kindly provided by Frank Bentzien, University Medical Center Eppendorf (UKE), Hamburg, Germany] and differentiated into macrophages by culturing them in RPMI-1640 (containing 100 units/ml penicillin, 100 µg/ml streptomycin, 2 mM glutamine and 20% autologous serum) at 37°C, 5% CO_2 and 90% humidity for a minimum of 7 days. Macrophages were detached by incubation of Accutase (Invitrogen, Waltham, MA) for at least 30 min in culturing conditions. The cells were collected, washed in PBS pH 7.3, resuspended in RPMI-1640 and seeded on 12-mm glass coverslips at a concentration of 100,000 cells per 100 µl medium. The cells were left to adhere for 1 h at culturing conditions. Then, 1 ml of RPMI-1640 (including antibiotics, glutamine and serum) was added, and cells were incubated for an additional 3 h.

Pharmacological treatments of cells

Cell were treated with the respective inhibitors after 4 h cultivation in RMPI-1640 (including antibiotics, glutamine and serum) by replacing the medium with new medium containing the respective drugs. The medium of the control cells was also replaced with new medium, containing the concentration of DMSO in which drugs were dissolved. Used drugs were (±)-blebbistatin (Merck Millipore, Billerica, MA) at a concentration of 10 µM for 30 min, as well as cytochalasin D (Merck Millipore) and ionomycin (Santa Cruz Biotechnology, Dallas, TX), which were both used at 2 µM for 10 min.

Immunofluorescence and microscopy

Cells were fixed for 10 min in 3.7% formaldehyde and permeabilized for 10 min in permabilization buffer (0.5% Triton-X-100, PBS pH 7.3). After staining the cells with antibodies or labelling reagents, the coverslips were mounted in Mowiol (Calbiochem, Darmstadt, Germany) containing DABCO (25 mg/ml; Sigma-Aldrich, St Louis, MO) as anti-fading reagent. Images of fixed samples were acquired with confocal laser-scanning microscope Leica DMI 6000 with a Leica TCS SP5 AOBS confocal point scanner equipped with an oil-immersion HCX PL APO CS 63×/1.4 NA objective and 2× HyD, 2× PMT detectors. Processing of images was performed with Volocity 6.1.1 software (Perkin Elmer, Waltham, MA) and Fiji (Schindelin et al., 2012).

Antibodies and reagents

F-actin was stained using AlexaFluor-568- and AlexaFluor-647-coupled phalloidin at a dilution of 1:50 (for Fig. 4) and 1:100 (for all other experiments) (Invitrogen). Rabbit anti-myosin IIA polyclonal antibody (pAb) (1:300) was purchased from Sigma-Aldrich. Rabbit-anti-LSP1 pAb (1:100) was purchased from Atlas Antibodies (Bromma, Sweden). Mouse anti-vinculin monoclonal antibody (mAb) (1:200) was purchased from Sigma-Aldrich. Fluorochrome-coupled secondary antibodies (all conjugated with either AlexaFluor-488 or AlexaFluor-568) were purchased from Life Technologies (Waltham, MA) and used at dilutions of 1:200.

Software, image and data processing and statistical analysis

The macro code for the semi-automatic analysis was written in Fiji (Schindelin et al., 2012). All data were processed using Excel 2013 (Microsoft, Redmond, WA) and GraphPad Prism 6 (La Jolla, CA). The podosome profile graph in Fig. 1 was processed using cubic spline interpolation. Statistical analysis included unpaired Student's *t*-tests with assumed Gaussian distribution for the graphs in Fig. 3. An *F*-test was additionally run to test for equal or unequal standard deviations. If standard deviations of the results were unequal, Student's *t*-test was performed with the Welch's correction. Representative micrographs in this paper are shown as original images with individual linear contrast enhancement for visibility. Images in Figs 1B3–6, 2A,B, 3A,B, 6A,B and 7A,C are shown as output of the Poji analysis and are thus modified copies from the original image.

Acknowledgements

We thank Frank Bentzien (UKE transfusion medicine) for buffy coats; Philippe Chavrier and Pedro Monteiro for providing invadopodia images for Poji analysis; Andrea Mordhorst for expert technical assistance; Kathrin Weber and Sven Hey for their help in validation of podosome detection; the UKE microscopy facility (UMIF) for help with microscopy and image analysis; and Alessandra Cambi and Martin Aepfelbacher for continuous support.

Competing interests

The authors declare no competing or financial interests.

Author contributions

Conceptualization: R.H., S.L.; Methodology: R.H., K.v.d.D., P.C., S.L.; Software: R.H., K.v.d.D.; Validation: R.H., K.v.d.D., S.L.; Formal analysis: R.H., P.C.; Investigation: S.L.; Resources: S.L.; Writing - original draft: R.H., S.L.; Writing - review & editing: R.H., K.v.d.D., S.L.; Visualization: R.H., P.C., S.L.; Supervision: S.L.; Project administration: S.L.; Funding acquisition: S.L.

Funding

This work is part of the doctoral thesis of R.H. and was supported by Deutsche Forschungsgemeinschaft [LI925/8-1 to S.L.].

Data availability

The Poji macro code, along with user guide and other supplementary files, is available from GitHub: https://github.com/roherzog/Poji.

Supplementary information

Supplementary information available online at
http://jcs.biologists.org/lookup/doi/10.1242/jcs.238964.supplemental

Peer review history

The peer review history is available online at
https://jcs.biologists.org/lookup/doi/10.1242/jcs.238964.reviewer-comments.pdf

References

Akisaka, T., Yoshida, H., Inoue, S. and Shimizu, K. (2001). Organization of cytoskeletal F-actin, G-actin, and gelsolin in the adhesion structures in cultured osteoclast. *J. Bone Miner. Res.* **16**, 1248-1255. doi:10.1359/jbmr.2001.16.7.1248

Albiges-Rizo, C., Destaing, O., Fourcade, B., Planus, E. and Block, M. R. (2009). Actin machinery and mechanosensitivity in invadopodia, podosomes and focal adhesions. *J. Cell Sci.* **122**, 3037-3049. doi:10.1242/jcs.052704

Alonso, F., Spuul, P., Daubon, T., Kramer, I. J. and Génot, E. (2019). Variations on the theme of podosomes: a matter of context. *Biochim. Biophys. Acta Mol. Cell Res.* **1866**, 545-553. doi:10.1016/j.bbamcr.2018.12.009

Berginski, M. E., Creed, S. J., Cochran, S., Roadcap, D. W., Bear, J. E. and Gomez, S. M. (2014). Automated analysis of invadopodia dynamics in live cells. *PeerJ* **2**, e462. doi:10.7717/peerj.462

Bhuwania, R., Cornfine, S., Fang, Z., Kruger, M., Luna, E. J. and Linder, S. (2012). Supervillin couples myosin-dependent contractility to podosomes and enables their turnover. *J. Cell Sci.* **125**, 2300-2314. doi:10.1242/jcs.100032

Burgstaller, G. and Gimona, M. (2005). Podosome-mediated matrix resorption and cell motility in vascular smooth muscle cells. *Am. J. Physiol. Heart Circ. Physiol.* **288**, H3001-H3005. doi:10.1152/ajpheart.01002.2004

Burns, S., Thrasher, A. J., Blundell, M. P., Machesky, L. and Jones, G. E. (2001). Configuration of human dendritic cell cytoskeleton by Rho GTPases, the WAS protein, and differentiation. *Blood* **98**, 1142-1149. doi:10.1182/blood.V98.4.1142

Cervero, P., Panzer, L. and Linder, S. (2013). Podosome reformation in macrophages: assays and analysis. *Methods Mol. Biol.* **1046**, 97-121. doi:10.1007/978-1-62703-538-5_6

Cervero, P., Wiesner, C., Bouissou, A., Poincloux, R. and Linder, S. (2018). Lymphocyte-specific protein 1 regulates mechanosensory oscillation of podosomes and actin isoform-based actomyosin symmetry breaking. *Nat. Commun.* **9**, 515. doi:10.1038/s41467-018-02904-x

Destaing, O., Saltel, F., Géminard, J.-C., Jurdic, P. and Bard, F. (2003). Podosomes display actin turnover and dynamic self-organization in osteoclasts expressing actin-green fluorescent protein. *Mol. Biol. Cell* **14**, 407-416. doi:10.1091/mbc.e02-07-0389

Destaing, O., Block, M. R., Planus, E. and Albiges-Rizo, C. (2011). Invadosome regulation by adhesion signaling. *Curr. Opin. Cell Biol.* **23**, 597-606. doi:10.1016/j.ceb.2011.04.002

El Azzouzi, K., Wiesner, C. and Linder, S. (2016). Metalloproteinase MT1-MMP islets act as memory devices for podosome reemergence. *J. Cell Biol.* **213**, 109-125. doi:10.1083/jcb.201510043

Evans, J. G., Correia, I., Krasavina, O., Watson, N. and Matsudaira, P. (2003). Macrophage podosomes assemble at the leading lamella by growth and fragmentation. *J. Cell Biol.* **161**, 697-705. doi:10.1083/jcb.200212037

Gimona, M., Kaverina, I., Resch, G. P., Vignal, E. and Burgstaller, G. (2003). Calponin repeats regulate actin filament stability and formation of podosomes in smooth muscle cells. *Mol. Biol. Cell* **14**, 2482-2491. doi:10.1091/mbc.e02-11-0743

Joosten, B., Willemse, M., Fransen, J., Cambi, A. and van den Dries, K. (2018). Super-resolution correlative light and electron microscopy (SR-CLEM) reveals novel ultrastructural insights into dendritic cell podosomes. *Front. Immunol.* **9**, 1908. doi:10.3389/fimmu.2018.01908

Kopp, P., Lammers, R., Aepfelbacher, M., Woehlke, G., Rudel, T., Machuy, N., Steffen, W. and Linder, S. (2006). The kinesin KIF1C and microtubule plus ends regulate podosome dynamics in macrophages. *Mol. Biol. Cell* **17**, 2811-2823. doi:10.1091/mbc.e05-11-1010

Kumari, S., Mak, M., Poh, Y.-C., Tohme, M., Watson, N., Melo, M., Janssen, E., Dustin, M., Geha, R. and Irvine, D. J. (2020). Cytoskeletal tension actively sustains the migratory T-cell synaptic contact. *EMBO J.* **39**, e102783. doi:10.15252/embj.2019102783

Labernadie, A., Thibault, C., Vieu, C., Maridonneau-Parini, I. and Charriere, G. M. (2010). Dynamics of podosome stiffness revealed by atomic force microscopy. *Proc. Natl. Acad. Sci. USA* **107**, 21016-21021. doi:10.1073/pnas.1007835107

Linder, S. (2007). The matrix corroded: podosomes and invadopodia in extracellular matrix degradation. *Trends Cell Biol.* **17**, 107-117. doi:10.1016/j.tcb.2007.01.002

Linder, S. and Wiesner, C. (2015). Tools of the trade: podosomes as multipurpose organelles of monocytic cells. *Cell. Mol. Life Sci.* **72**, 121-135. doi:10.1007/s00018-014-1731-z

Linder, S., Nelson, D., Weiss, M. and Aepfelbacher, M. (1999). Wiskott-Aldrich syndrome protein regulates podosomes in primary human macrophages. *Proc. Natl. Acad. Sci. USA* **96**, 9648-9653. doi:10.1073/pnas.96.17.9648

Linder, S., Higgs, H., Hüfner, K., Schwarz, K., Pannicke, U. and Aepfelbacher, M. (2000). The polarization defect of Wiskott-Aldrich syndrome macrophages is linked to dislocalization of the Arp2/3 complex. *J. Immunol.* **165**, 221-225. doi:10.4049/jimmunol.165.1.221

Linder, S., Wiesner, C. and Himmel, M. (2011). Degrading devices: invadosomes in proteolytic cell invasion. *Annu. Rev. Cell Dev. Biol.* **27**, 185-211. doi:10.1146/annurev-cellbio-092910-154216

Liu, C. and Hermann, T. E. (1978). Characterization of ionomycin as a calcium ionophore. *J. Biol. Chem.* **253**, 5892-5894.

Luxenburg, C., Geblinger, D., Klein, E., Anderson, K., Hanein, D., Geiger, B. and Addadi, L. (2007). The architecture of the adhesive apparatus of cultured osteoclasts: from podosome formation to sealing zone assembly. *PLoS ONE* **2**, e179. doi:10.1371/journal.pone.0000179

Maupin, P., Phillips, C. L., Adelstein, R. S. and Pollard, T. D. (1994). Differential localization of myosin-II isozymes in human cultured cells and blood cells. *J. Cell Sci.* **107**, 3077-3090.

Meddens, M. B. M., Rieger, B., Figdor, C. G., Cambi, A. and van den Dries, K. (2013). Automated podosome identification and characterization in fluorescence microscopy images. *Microsc. Microanal.* **19**, 180-189. doi:10.1017/S1431927612014018

Miyauchi, A., Hruska, K. A., Greenfield, E. M., Duncan, R., Alvarez, J., Barattolo, R., Colucci, S., Zambonin-Zallone, A., Teitelbaum, S. L. and Teti, A. (1990). Osteoclast cytosolic calcium, regulated by voltage-gated calcium channels and extracellular calcium, controls podosome assembly and bone resorption. *J. Cell Biol.* **111**, 2543-2552. doi:10.1083/jcb.111.6.2543

Monteiro, P., Rossé, C., Castro-Castro, A., Irondelle, M., Lagoutte, E., Paul-Gilloteaux, P., Desnos, C., Formstecher, E., Darchen, F., Perrais, D. et al. (2013). Endosomal WASH and exocyst complexes control exocytosis of MT1-MMP at invadopodia. *J. Cell Biol.* **203**, 1063-1079. doi:10.1083/jcb.201306162

Moreau, V., Tatin, F., Varon, C. and Genot, E. (2003). Actin can reorganize into podosomes in aortic endothelial cells, a process controlled by Cdc42 and RhoA. *Mol. Cell. Biol.* **23**, 6809-6822. doi:10.1128/MCB.23.19.6809-6822.2003

Murphy, D. A. and Courtneidge, S. A. (2011). The 'ins' and 'outs' of podosomes and invadopodia: characteristics, formation and function. *Nat. Rev. Mol. Cell Biol.* **12**, 413-426. doi:10.1038/nrm3141

Murphy, D. A., Diaz, B., Bromann, P. A., Tsai, J. H., Kawakami, Y., Maurer, J., Stewart, R. A., Izpisúa-Belmonte, J. C. and Courtneidge, S. A. (2011). A Src-Tks5 pathway is required for neural crest cell migration during embryonic development. *PLoS ONE* **6**, e22499. doi:10.1371/journal.pone.0022499

Panzer, L., Trübe, L., Klose, M., Joosten, B., Slotman, J., Cambi, A. and Linder, S. (2016). The formins FHOD1 and INF2 regulate inter- and intra-structural contractility of podosomes. *J. Cell Sci.* **129**, 298-313. doi:10.1242/jcs.177691

Paterson, E. K. and Courtneidge, S. A. (2018). Invadosomes are coming: new insights into function and disease relevance. *FEBS J.* **285**, 8-27. doi:10.1111/febs.14123

Proag, A., Bouissou, A., Vieu, C., Maridonneau-Parini, I. and Poincloux, R. (2016). Evaluation of the force and spatial dynamics of macrophage podosomes by multi-particle tracking. *Methods* **94**, 75-84. doi:10.1016/j.ymeth.2015.09.002

Sampath, P. and Pollard, T. D. (1991). Effects of cytochalasin, phalloidin and pH on the elongation of actin filaments. *Biochemistry* **30**, 1973-1980. doi:10.1021/bi00221a034

Schindelin, J., Arganda-Carreras, I., Frise, E., Kaynig, V., Longair, M., Pietzsch, T., Preibisch, S., Rueden, C., Saalfeld, S., Schmid, B. et al. (2012). Fiji: an open-source platform for biological-image analysis. *Nat. Methods* **9**, 676-682. doi:10.1038/nmeth.2019

Teti, A., Blair, H. C., Schlesinger, P., Grano, M., Zambonin-Zallone, A., Kahn, A. J., Teitelbaum, S. L. and Hruska, K. A. (1989). Extracellular protons acidify osteoclasts, reduce cytosolic calcium, and promote expression of cell-matrix attachment structures. *J. Clin. Invest.* **84**, 773-780. doi:10.1172/JCI114235

van den Dries, K., Meddens, M. B., de Keijzer, S., Shekhar, S., Subramaniam, V., Figdor, C. G. and Cambi, A. (2013a). Interplay between myosin IIA-mediated contractility and actin network integrity orchestrates podosome composition and oscillations. *Nat. Commun.* **4**, 1412. doi:10.1038/ncomms2402

van den Dries, K., Schwartz, S. L., Byars, J., Meddens, M. B. M., Bolomini-Vittori, M., Lidke, D. S., Figdor, C. G., Lidke, K. A. and Cambi, A. (2013b). Dual-color superresolution microscopy reveals nanoscale organization of mechanosensory podosomes. *Mol. Biol. Cell* **24**, 2112-2123. doi:10.1091/mbc.e12-12-0856

van den Dries, K., Bolomini-Vittori, M. and Cambi, A. (2014). Spatiotemporal organization and mechanosensory function of podosomes. *Cell Adh. Migr.* **8**, 268-272. doi:10.4161/cam.28182

van den Dries, K., Linder, S., Maridonneau-Parini, I. and Poincloux, R. (2019). Probing the mechanical landscape - new insights into podosome architecture and mechanics. *J. Cell Sci.* **132**, jcs236828. doi:10.1242/jcs.236828

Yoshio, T., Morita, T., Kimura, Y., Tsujii, M., Hayashi, N. and Sobue, K. (2007). Caldesmon suppresses cancer cell invasion by regulating podosome/invadopodium formation. *FEBS Lett.* **581**, 3777-3782. doi:10.1016/j.febslet.2007.06.073

Zambonin-Zallone, A., Teti, A., Grano, M., Rubinacci, A., Abbadini, M., Gaboli, M. and Marchisio, P. C. (1989). Immunocytochemical distribution of extracellular matrix receptors in human osteoclasts: a β3 integrin is colocalized with vinculin and talin in the podosomes of osteoclastoma giant cells. *Exp. Cell Res.* **182**, 645-652. doi:10.1016/0014-4827(89)90266-8

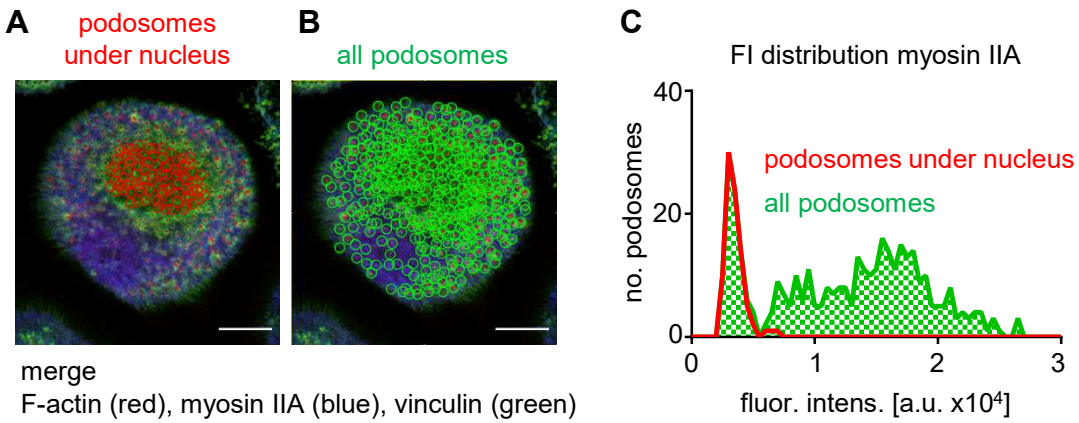

Fig. S1 Distribution of mysoin IIA at podosomes. (A,B) Confocal micrographs of the control cell of Fig. 2, merge from F-actin (red, phalloidin-AlexaFluor-647), myosin IIA (blue) and vinculin (green), both stained by using primary and fluorescently labeled secondary antibodies (AlexaFluor-568 for myosin IIA and AlexaFluor-488 for vinculin). Podosomes that are localized underneath the nucleus (red circles) **(A)**) and in entire cell area (green circles) are marked respectively **(B)**. Bars: 10 µm. **(C)** Fluorescence intensity distribution. Podosomes were binned in groups with a fluorescence intensity (FI) interval of 500 a.u.; number of podosomes inside groups was plotted against the intensity for all podosomes (green line with dashed area under the curve; compare with blue graph in Fig. 2C) and for podosomes under the nucleus only (red line).

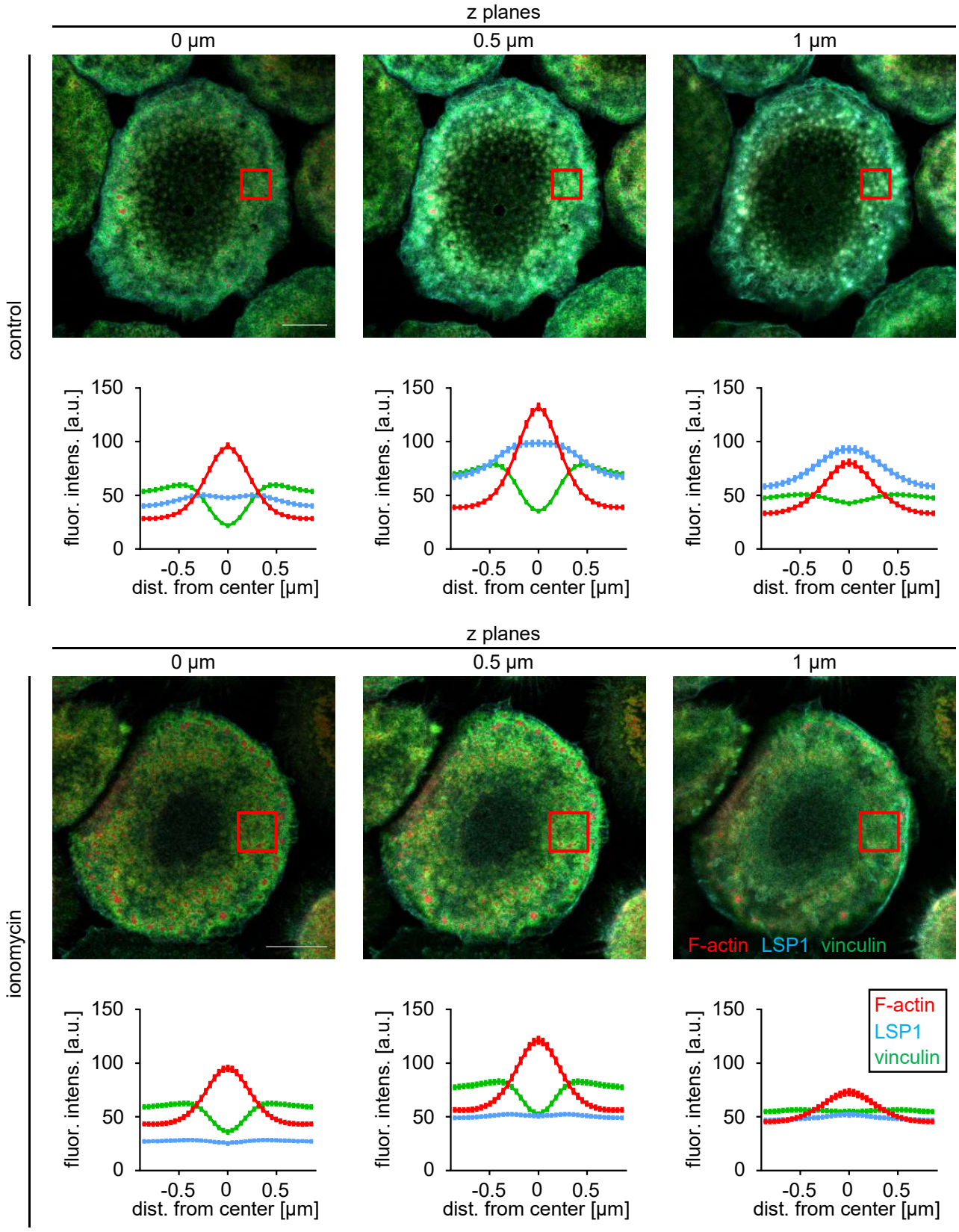

Fig. S2 Whole cells from detailed ROIs of Fig. 4. Confocal micrographs and profile analyses of whole cells, with red squares indicating the areas shown as detailed ROIs in Fig. 4. Upper row: control cell, lower row: ionomycin-treated cell. Both cells are shown in three focal planes (z=0, 0.5 and 1 µm), as merges of F-actin (red, phalloidin-AlexaFluor-647), LSP1 (cyan) and vinculin (green), both stained by using primary and fluorescently labeled secondary antibodies (AlexaFluor-568 for LSP1 and AlexaFluor-488 for vinculin). Bars: 10 µm. The respective profile analyses are shown for the three proteins F-actin, LSP1 and vinculin as mean of all podosomes with SEM. n=468 podosomes (control) and n=383 podosomes (ionomycin).